Multiphysics Modelling of Powder Coating of U-Profiles: Towards Simulation-based Optimization of Key-Performance Attributes by Variation of Powder-Parameters

G Boiger[1]*, B Siyahhan[1], AS Fallah[2], H Khawaja[3], M Moatamedi[4]

1. ICP Institute of Computational Physics, ZHAW Zurich University of Applied Sciences, Technikumstrasse 71, 8400 Winterthur, Switzerland

2. Department of Machinery, Electronics and Chemistry, Oslo Metropolitan University, Pilestredet 35, 0166 Oslo, Norway

3. Department of Automation and Process Engineering, Faculty of Engineering Science and Technology, UiT The Arctic University of Norway, Tromsø, Norway

4. New York University London, London, United Kingdom

ABSTRACT

Multiphysics simulation software has been developed to predict the key performance attributes of industrial powder coating applications based on applied process-parameter settings. The software is a Eulerian-Lagrangian finite-volume Multiphysics solver based on OpenFOAM, capable of modelling mass transfer effects between powder-coating pistols and electrically grounded metallic substrates. It considers various factors such as fluid dynamics of process airflow, coating-particle dynamics, particle-substrate interactions, and particle charging mechanisms within the corona. The software is fully compatible with Massive Simultaneous Cloud Computing technology, allowing hundreds of simulated coating scenarios to be computed simultaneously. Experimental validation efforts have been conducted, indicating a high degree of practical relevance of the technology.

The current simulation study aims to demonstrate the potential of the simulation software for adjusting coating lines and optimizing powder coating of U-profiles. Specifically, the study focuses on optimizing the key-performance-attributes of the powder coating application with respect to varying material parameters of the applied powder, namely mean particle diameter, standard deviation of Gaussian particle size distribution, and powder particle density. The software predicts and visualizes coating patterns, coating efficiencies, and the batch-based standard deviation of coating thickness on a U-shaped metallic substrate, resulting in concrete and optimized powder settings. The presented results and the applied software are highly relevant for powder material suppliers.

*Corresponding Author: gernot.boiger@zhaw.ch

1. INTRODUCTION

1.1. Industrial Powder Coating

While the process of industrial wet paint coating still dominates the coating sector, powder coating is described as emerging technology and accounted for approximately 15% of US coating market share in 2021, at a projected CAGR of 6.2% during 2021-2028 (see [23]). While both wet paint coating as well as powder coating use resins, additives, and pigments, powder coating eliminates the need for liquid solvents. Thus, powder coating reduces ecological impacts as compared to the more commonly used wet paint coating process (see [22]).

During the powder coating procedure, polymer particles are injected into the primary process airflow within a coating pistol. A high-voltage electrode is mounted towards the tip of the coating pistol. It forms an electrostatic field with an electrically grounded metallic substrate and ionizes process-air-oxygen to O^{2-} ions, forming a corona in its immediate vicinity. As the particles are transported through the corona, ions attach to the surfaces of the particles and charge them electrically.

Impacted by fluid-friction, electrostatic forces, and gravity, the charged powder particles protrude out of the coating pistol, across the coating chamber, towards the substrate surface, where they either stick, travel across the surface, or get blown off.

Key-performance-attributes of the powder coating process include i) shape of coating patterns, ii) coating homogeneity and iii) coating efficiency. These attributes vary with respect to a series of geometric-, process- and material parameters, some of which include: i) substrate geometry, ii) pistol-substrate distance and orientation, iii) applied- and effective voltage, iv) primary- (within coating pistol) and secondary- (at coating chamber inlet) process air flows, v) particle injection rate, vi) number and position of coating pistols, vii) kinetic pistol parameters, vi) ambient temperature and humidity, vii) mean powder particle diameter, viii) standard deviation of powder particle diameters, ix) powder particle -density, -material, and -shape as well as x) powder particle charge-function-coefficients.

In light of this ample array of degrees of freedom, the adjustment of coating lines to varying process parameters, such as i) environmental factors, ii) substrate geometry or iii) powder formulation, poses considerable challenges. Up to this day such coating-line adjustments are conducted based on empirical know-how and/or resource-intensive trial- and error schemes. This work proposes an alternative methodology for adjusting process lines. The proposed method is based on Multiphysics simulation-informed decisions.

1.2. The Multiphysics Powder Coating Simulation Solver

The development of the Multiphysics powder coating simulation solver aimed to enhance the efficiency and quality of the coating-line-adjustments while reducing resource intensity. This software is based on an Eulerian-Lagrangian finite-volume solver and has been developed using the open-source CFD toolbox OpenFOAM [1] over a period of 15 years. Initially developed for automotive filtration applications [11-21], it has evolved into a versatile simulator for particle-laden flows, specifically designed for modelling coating applications [2-5]. The model has been validated [2] and is now capable of simulating all relevant mass transfer phenomena within the powder coating process, including the motion of Lagrangian coating particles within the Eulerian process airflow field, past the high voltage electrode,

across the coating chamber and towards either a substrate or any outlet vent. It considers various phenomena, such as fluid dynamics of process-air, electrostatic field between high-voltage electrode and substrate, particle-dynamics (including fluid-particle, particle-particle-, particle-electro-, and detailed particle-substrate interaction), corona formation and spreading, and particle charging kinetics. Thus, the software can predict the key performance attributes of a powder coating process, such as coating pattern shapes, coating efficiency, and coating homogeneity, with respect to applied process- and material parameters. The software has recently become fully compatible with Massive Simultaneous Cloud Computing technology [6-10], allowing hundreds of coating-process-parameter scenarios to be predicted within a reasonable working and waiting time. This capability was extensively used in the study presented here.

1.3. Study Focus: Investigating the Impact of varying Powder Parameters on Coating of U-profiles

The purpose of this study is twofold: Firstly, to demonstrate the capacity and potential of the software to be at the basis of a simulation-informed methodology for adjusting coating lines. Secondly to provide concrete input for optimizing one exemplary, industrially very relevant

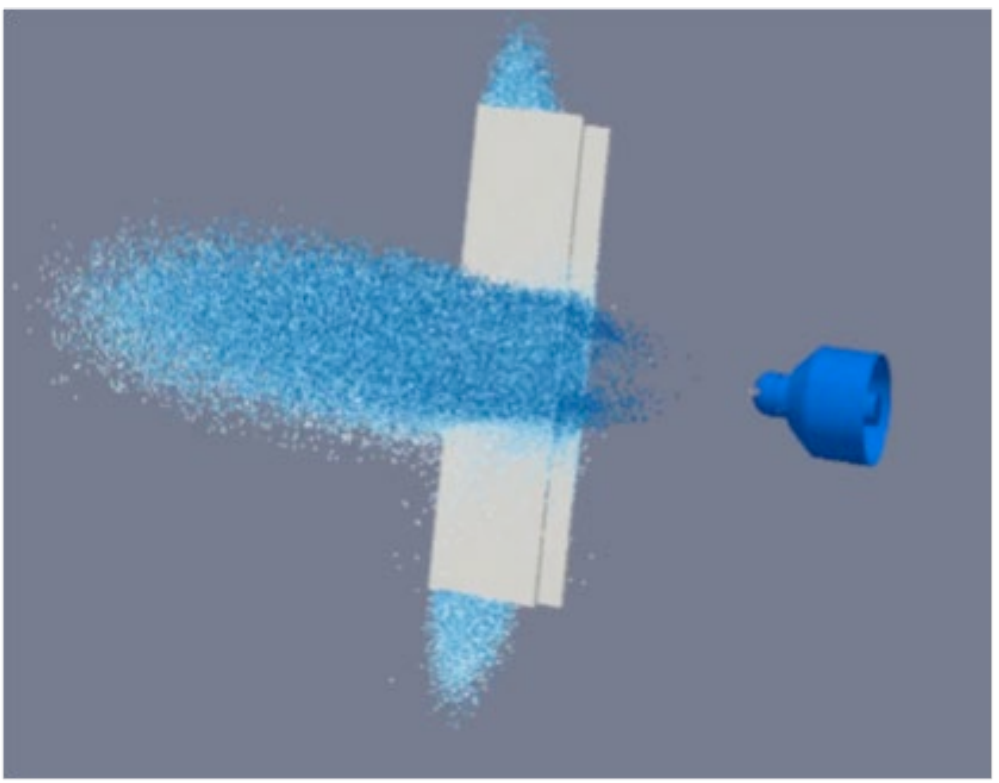

Figure 1. Simulated powder coating process of a metallic U-profile. The simulated Lagrangian particle cloud (light blue) of approximately 250k particles is visualised as it leaves the coating pistol (dark blue, right), engulfs the U-profile (grey, centre), partly sticks to- and partly passes the substrate.

scenario: the single-pistol, static (= pistol is immobile) powder coating of an electrically grounded, U-shaped metallic substrate (U-profile). Thereby pistol and substrate are placed within a hexahedral coating chamber featuring inlet- and outlet vents upstream and downstream of the pistol - U-profile set-up. The pistol - U-profile configuration is shown in Figure 1 along with a snapshot of an evolving powder coating particle cloud.

The specific focus of this study lies on the impact of powder material parameters on the key-performance-attributes of the coating of U-profiles. Exploiting the benefits of Massive Simultaneous Cloud Computing, large batches of simulation runs were conducted and automatically evaluated in the cloud. Thus, the impact of varying i) mean particle diameters, ii) standard deviation of Gaussian particle-size distribution and iii) particle density on the coating outcome was investigated. Hereby the coating outcome was explicitly defined as i) qualitative shape of coating patterns, ii) coating efficiencies, iii) average coating thicknesses, and iv) coating homogeneity. The obtained result can now serve as basis for knowledge-based optimization of the powder quality for U-profile applications. While the specific results of the mean powder particle diameter variation were already thoroughly laid out in [27], this article extends the findings to varying i) the standard deviation of Gaussian particle size distribution and to varying ii) particle densities.

2. METHODS: NUMERICAL MODEL AND CLOUD COMPUTING

2.1. The Solver: Capabilities

The physical and numerical simulation model used in this study is based on previous work by the authors (references [2], [5], and [24]). As mentioned in [27], the model includes several key aspects such as: i) Reynolds Average Stress (RAS) modelling of process-air-flow turbulence, ii) an empirical approach to account for localized turbulence effects on particle motion [25], iii) a steady-state Maxwell equations solver to model the electrostatic field between a high-voltage electrode and a grounded substrate, iv) modelling of the particle-laden flow inside the powder-coating-pistol, v) Lagrangian modelling of several hundred-thousand coating particles to represent the specific powder cloud per application case, vi) a detailed consideration of fluid-particle-, mechanical-, and electrical particle-particle- and particle-substrate interaction, vii) modelling of spreading of ionized oxygen in the vicinity of the high-voltage electrode (= corona formation) [24], viii) semi-empirical modelling of particle charging and substrate deposition mechanisms.

The model was recently extended to include: i) multiple coating pistols simultaneously, ii) user-defined particle injection functions, iii) user-defined pistol-motion functions, and to include the capability for iv) converting Lagrangian-particle-based, discrete coating patterns into continuous coating thickness fields (coating volume fractions). Although extensions i), ii), and iii) are not demonstrated in this study, extension iv) is important for comparing and validating simulation-based predictions against real-life coating patterns (as described in section 3.3) and evaluating process-parameter scenarios.

2.2. The Solver: Result Evaluation

In order to evaluate and compare simulated coating process scenarios, numerical indicators are computed: i) the volume fraction field, ii) the coating efficiency, and iii) the standard batch-based coating thickness deviation.

2.2.1. Volume fraction field:

The introduction of the volume fraction field v_f achieves the translation from discrete local particle counts on substrate surfaces to a continuous coating thickness field. It relates the sum of volumes of all i-indexed coating particles $V_{Pc,j,i}$ within each hexahedral finite-volume cell j to the volume of the cell $V_{C,j}$ as seen in Eqn. 1. The volume fraction field is essential for qualitative visual evaluation of numerically predicted coating patterns. However, it does require uniform grid spacing at the surface of the substrate for inter-case- or inter-substrate-comparability.

$$v_{f,j} = \frac{\sum_i V_{Pc,j,i}}{V_{C,j}} \quad \text{(Eqn.1)}$$

2.2.2. Coating efficiency:

The total coating efficiency $E(-)$ is computed as the ratio of particle volume ultimately sticking to the substrate surface V_{Pc} to total injected particle volume V_{Pinj}. In addition, substrate-surface-batch-specific coating efficiency $E_k(-)$ is evaluated for each surface batch k. It relates the coated particle volume $V_{Pc,k}$ per surface-batch to the total injected particle volume according Eqn.2.

$$E_k = \frac{V_{Pc,k}}{V_{Pinj}} \quad \text{(Eqn.2)}$$

2.2.3. Standard batch-based coating thickness deviation (SCD):

The standard batch-based coating thickness deviation σ_c is one of many possible measures to indicate coating (in-) homogeneity. It compares the substrate-surface-batch-specific coating efficiencies E_k to the average substrate-surface-batch coating efficiency $E_{k,avg}$ applying a batch-surface-specific weighting factor w_k according to Eqn.3. The relative standard batch-based coating thickness deviation (RSCD), $\sigma_{c,rel}$ is then defined as the ratio of SCD to $E_{k,avg}$ according to Eqn.4

$$\sigma_c = \sqrt{\frac{\sum_k^n [w_k (E_k - E_{k,avg})]^2}{n}} \quad \text{(Eqn.3)}$$

$$\sigma_{c,rel} = \frac{\sigma_c}{E_{k,avg}} \quad \text{(Eqn.4)}$$

2.3. Solver Validation on Flat Plate- and U-Profile Substrates

2.3.1. Qualitative and Quantitative Solver Validation on Flat Plate Substrates

In [2], a quantitative validation of the solver was conducted based on variations in process parameters for the powder-coating of numerous metallic flat plate substrates. The validation compared coating patterns (see Figure 2 for a qualitative example), coating efficiencies, and relative coating volumes between simulated and measured results. The process parameters varied included applied voltage, volumetric process airflow rate, pistol-substrate distance, and pistol-substrate orientation.

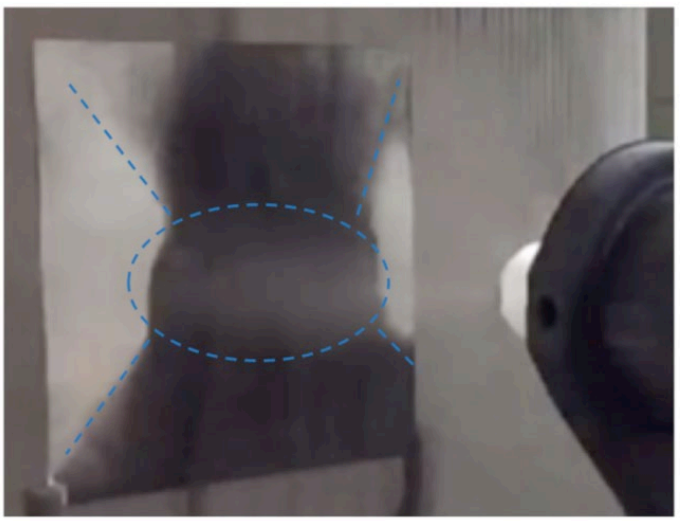

(a)

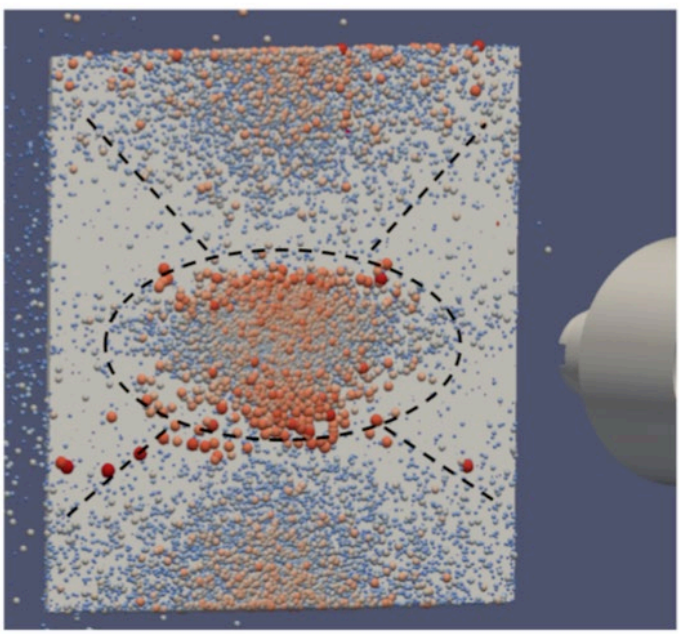

(b)

Figure 2. Example of qualitative correspondence of observed (a) and simulated (b) deposition patterns. Here particles were deposited on the front side of a $10cm\ x\ 10cm$ metallic-plate substrate. Process parameters: Effective voltage $U_{eff} = 30kV$, Pistol-to-substrate distance $D = 20cm$; Primary process airflow rate $Q_1 = 3m^3/h$; Secondary process airflow rate $Q_2 = 0.5m^3/h$; Coating duration experiment/simulation: single-particle-burst $t = 1.0\ sec$.

The validation study in [2] was also extended to larger metallic substrates, including single-particle-burst coating experiments on dozens of metallic A4 plates. Figure 3 provides an example of the single-particle-burst coating of an A4 plate, with a focus on the window-frame-effect. This phenomenon describes the tendency for more thickly coated regions to occur towards the edges of substrates. The comparison showed that the solver accurately predicts the occurrence of window frames by the bottom edge of the substrate.

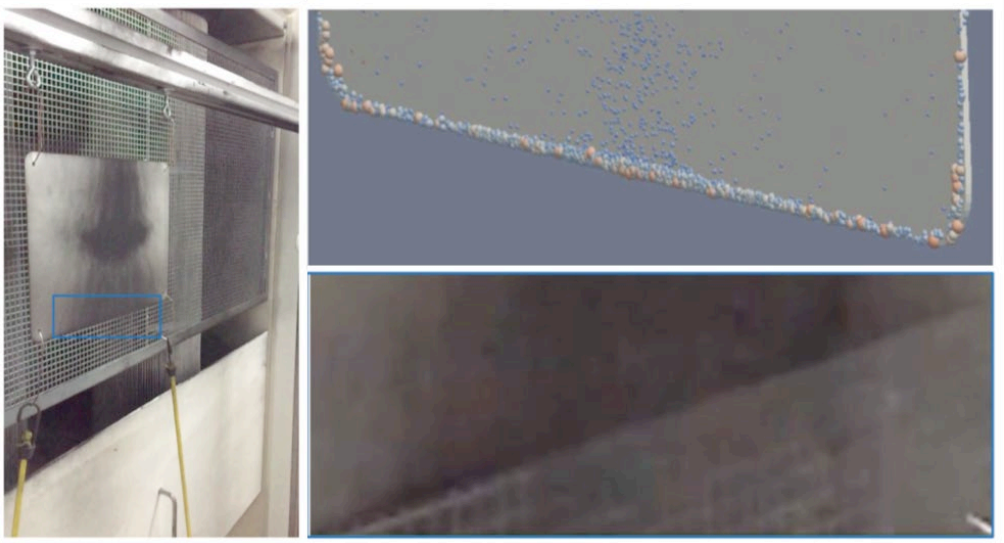

Figure 3. Example of qualitative correspondence of observed (left, bottom-right) and simulated (top-right) deposition patterns. Here particles were deposited on the front side of an A4 metallic-plate substrate (left). The images on the right focus on the bottom edge of the A4 plate, where regions of thicker coating window frames occur both in the experiment as well as in the simulation–based prediction. Process parameters: Effective voltage $U_{eff} = 30kV$, pistol-to-substrate distance $D = 20cm$; Primary process airflow rate $Q_1 = 3m^3/h$; Secondary process airflow rate $Q_2 = 0.5m^3/h$; Coating duration experiment/simulation: single-particle-burst $t = 1.0\ sec$.

2.3.2. Qualitative Validation on U-Profile Substrates

U-profiles are among the most commonly coated substrate classes in the powder coating industry. Thus, in the course of this study, the solver was explicitly applied to the powder coating of metallic U-profile substrates. Figure 4 demonstrates the temporal evolution of one such Eulerian-Lagrangian simulation as a cloud of some 250k particles engulfs, partly sticks to, and partially passes a U-profile substrate.

Qualitative validation efforts of the solver were extended to the simulation of U-profile coating applications. Therefore a metallic U-profile was powder-coated under controlled experimental conditions within a lab coating chamber. A numerical simulation was run in order to replicate the same scenario, albeit in the time frame of a single-particle-burst

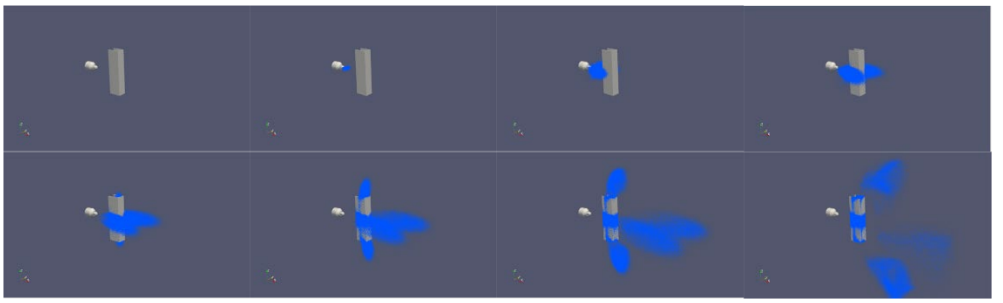

Figure 4. Demonstration of the evolution of a single-particle-burst powder coating simulation applied to a metallic U-profile. Earliest time: top-left; latest time: bottom-right. The simulated Lagrangian particle cloud (blue) of approximately 250k particles is visualised as it leaves the coating pistol (grey, left), engulfs the U-profile (grey, right), partly sticks to and partly passes the substrate.

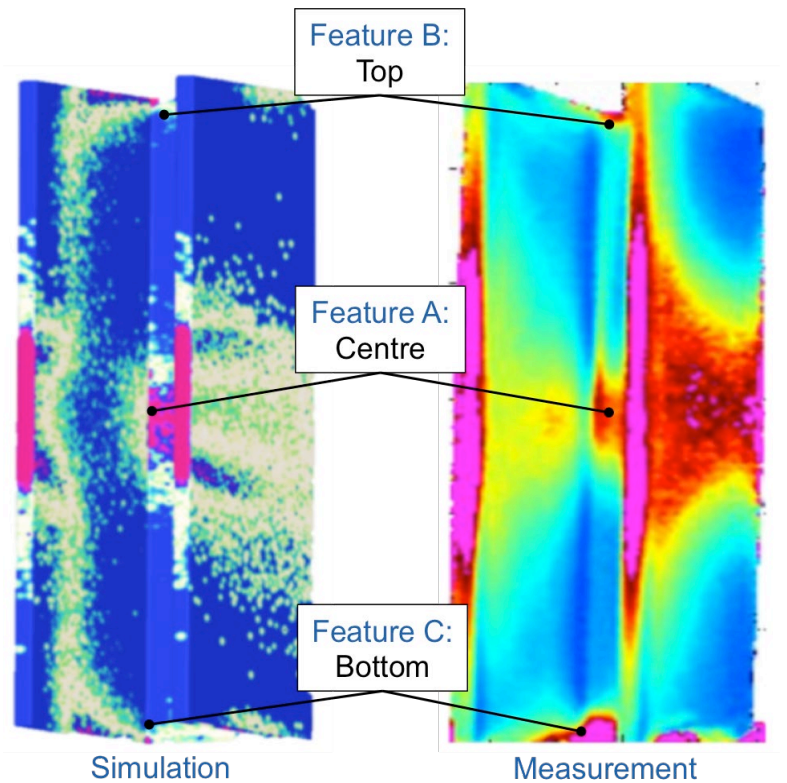

Figure 5a. Simulation based prediction (left) vs. experimentally derived (right) coating pattern of a powder coated U-profile. Process parameters: Effective voltage: $U_{eff} = 50kV$, Pistol-to-substrate distance $D = 15cm$; Primary process airflow rate $Q_1 = 2m^3/h$; Secondary process airflow rate $Q_2 = 0.5m^3/h$; Coating duration experiment/simulation: single-particle-burst $t = 1.0\,sec$; Mean particle diameter $D_{mean} = 34\mu m$; Standard deviation of particle diameters in Gaussian particle size distribution $\sigma = +/-16\mu m$; Particle density: $\rho = 1400\,kg/m^3$. Highlighted coating pattern features: A – Centre, B – Top and C – Bottom; See also [27].

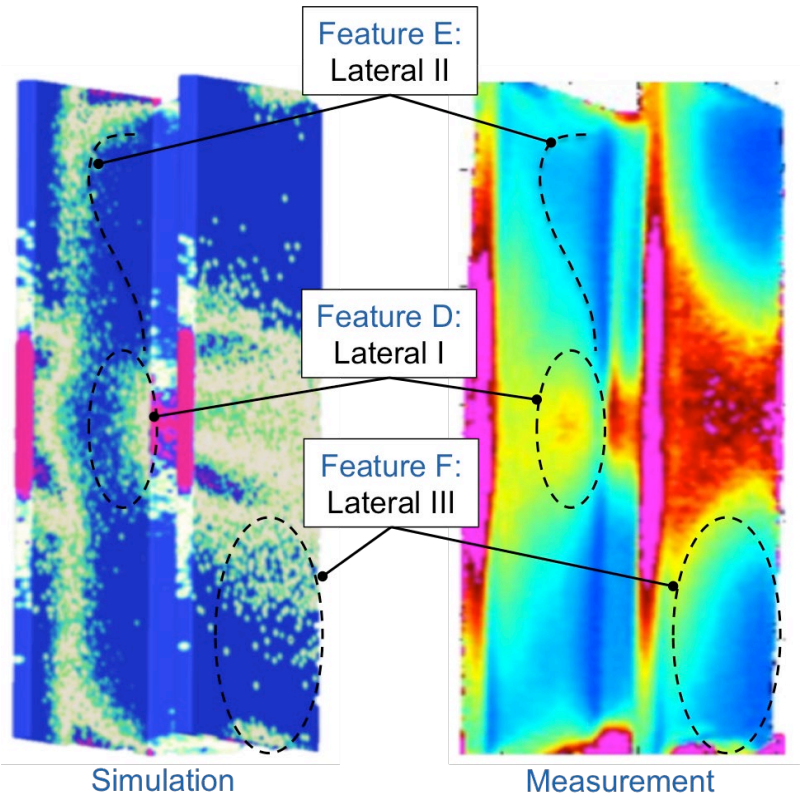

Figure 5b. Simulation-based prediction (left) vs. experimentally derived (right) coating pattern of a powder-coated U-profile. Process parameters: Effective voltage $U_{eff} = 50kV$, Pistol-to-substrate distance $D = 15cm$; Primary process airflow rate $Q_1 = 2m^3/h$; Secondary process airflow rate $Q_2 = 0.5m^3/h$; Coating duration experiment/simulation: single-particle-burst $t = 1.0\,sec$; Mean particle diameter $D_{mean} = 34\mu m$; Standard deviation of particle diameters in Gaussian particle size distribution $\sigma = +/-16\mu m$; Particle density: $\rho = 1400\,kg/m^3$. Highlighted coating pattern features: D – Lateral I, E – Lateral II, and F – Lateral III; See also [27].

application (1.0 sec real time). The powder coated U-profile was measured using Coatmaster-3D [26] technology such that the coating-thickness pattern after a single-particle-burst could be qualitatively compared to the simulation. A corner stone for being able to compare measured against computed results, was the visualization of the numerically retrieved coating pattern on the basis of the computed volume fraction field (see section 2.1). Note that the introduction of the visualized volume fraction field bridges the gap between particle-based Lagrangian simulation and field-based coating thickness data. Qualitative comparisons of the real-life- and the simulated coating case are shown in Figure 5a and Figure 5b. These are the main findings from these qualitative comparisons:

Feature A – Centre (see Figure 5a): The simulation manages to correctly predict the occurrence of a strongly coated region by the centre of the U-profile substrate as well as on the front-facing surfaces of both lateral protrusions.

Feature B – Top (see Figure 5a): The simulation manages to correctly predict the occurrence of a strongly coated region by the upper edge of the U-profile substrate (top window-frame).

Feature C – Bottom (see Figure 5a): The simulation manages to correctly predict the occurrence of a strongly coated region by the lower edge of the U-profile substrate (bottom window-frame).

Feature D – Lateral I (see Figure 5b): While the simulation correctly predicts the occurrence of a strongly coated region by the central foot of the inner, lateral protrusions of the U-profile substrate, its shape slightly differs from the measurement. Bearing in mind that measurement errors cannot be excluded, the simulated results are actually more plausible in this case than the measured ones, since they point to a higher coating density towards the inner edge.

Feature E – Lateral II (see Figure 5b): The simulation manages to predict the occurrence of a coating pattern, shaped like a distorted S, from the centre towards the upper and lower edges of the inner, lateral protrusions of the U-profile substrate, concurring with the measured results.

Feature F – Lateral III (see Figure 5b): While the simulation manages to roughly approximate the coating pattern at the outer lateral protrusions of the U-profile substrate, the shape does noticeably differ from measured results. A simple explanation for the observed deviations can be offered by considering the high result sensitivity at the outer lateral surfaces of the geometry. These very surfaces are oriented in parallel to the streamlines of the main process airflow. Thus, the coating patterns in these regions are highly sensitive to smallest changes in relative pistol-substrate orientation.

2.4. MSCC Massive Simultaneous Cloud Computing

The simulation software has been made fully compatible with the Kaleidosim cloud-computing platform [6-8], which has been gaining traction in accelerating workflows of extensive simulation studies [9-10]. Massive Simultaneous Cloud Computing (MSCC) capability has been established by integrating Kaleidosim API-functionality into the coding. This means that the user can now conduct extended (process-) parameter sweeps of up to 500 simulation cases to be run simultaneously on as many cloud-based computers. As a result, working- and waiting time to conduct computationally very expensive parameter studies, optimization runs or ensemble computing in general, can be dramatically decreased. Likewise, the capacity and extent of such studies can be notably increased at comparable working-/waiting time. The MSCC workflow was implemented and applied throughout this study, dramatically increasing sampling intensity within the vast U-profile powder-coating-parameter-space. Figure 6 depicts an overview of the MSCC workflow as applied to OpenFOAM based simulation runs.

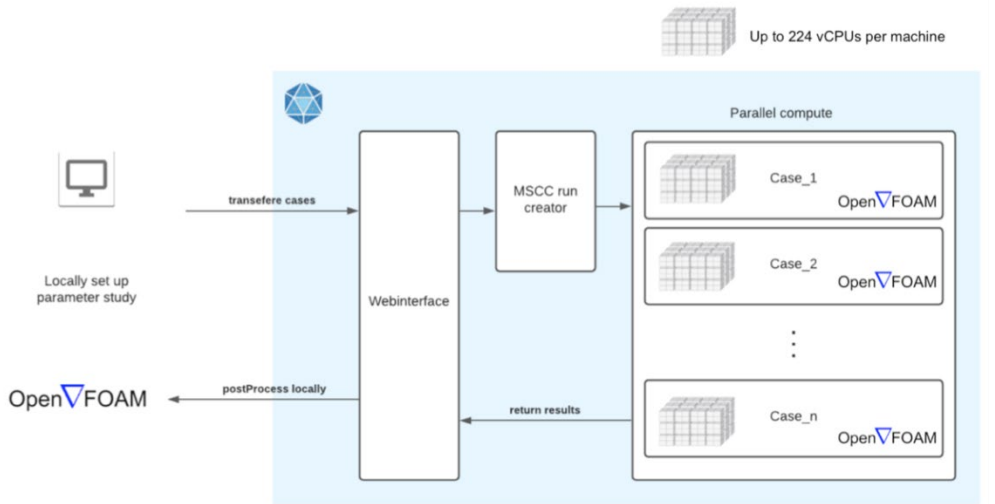

Figure 6. Overview of Massive Simultaneous Cloud Computing workflow as provided by Kaleidosim cloud platform, specifically for OpenFOAM-based numerical simulation runs. The workflow proves specifically efficient for parameter-sweeps where one single base-case is prepared locally, uploaded to a web-interface, multiplied within the MSCC run creator to represent up to 500 process-parameter combinations, then run on up to 500 cloud machines simultaneously with results being selectively either post-processed in the cloud or downloaded via a web-interface.

3. RESULTS

In the core-part of this study the simulation model was set to predict the impact of varying powder material parameters on the coating result of coated U-profiles. The varied powder material parameters were:

- Mean particle diameters (section 4.1);
- Standard deviation of particle diameters (section 4.2);
- Particle density (section 4.3);

In this context, the solver was set to represent the coating results in terms of the following key-performance-attributes:

- The Volume fraction field (see Eqn.1) represents visualized, predicted 3D coating patterns;
- The Coating efficiency (see Eqn.2) represents the predicted effective coating powder particle volume fraction;
- The Standard batch-based coating deviation (see Eqn. 3) represents the predicted coating homogeneity;

For each of the three powder parameters to-be-varied, a considerably large computational parameter study was conducted. Each study encompassed 100 individual simulation runs, where each key-performance-attribute was evaluated per simulation run.

Note that due to the employment of Massive Simultaneous Cloud Computing technology, each study only consumed approximately 120% of the wall-clock-time of one single simulation run.

3.1. Predicting the Impact of varying Powder Material Parameters: Mean particle diameter

This section presents the results of simulation-based predictions of the impact of varying Mean particle diameters D_p on i) coating patterns (see Figure 7a, 7b and 7c), ii) Coating Efficiencies (see Figure 8, blue) and iii) Relative Standard batch-based coating deviation (see Figure 8, green) of a powder coated U-profile substrate. While Mean particle diameters were varied in 100 steps between $5\mu m$ and $205\mu m$, process- and material-parameters were fixed as follows: applied voltage: $50kV$, distance pistol-substrate: 15cm, process airflow rate: $2m^3/h$, Standard deviation of particle diameters in Gaussian particle size distribution: $+/-16\mu m$; Particle density: $1400\ kg/m^3$.

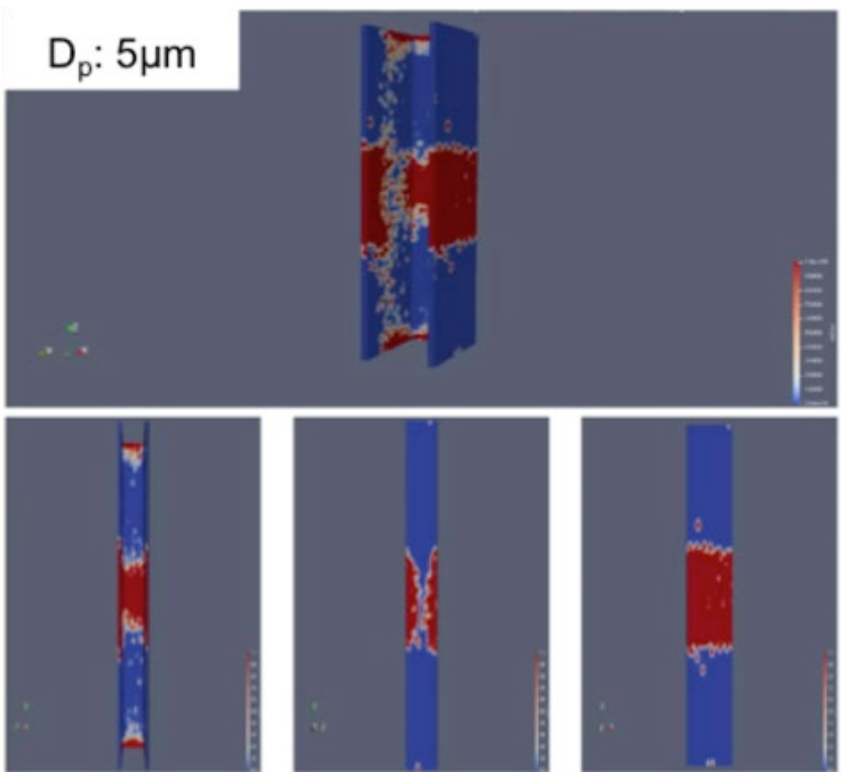

Figure 7a. Simulated coating patterns (visualization of Volume fraction fields) after single-burst-powder application for Mean particle diameter: 5µm. Top row shows front-side view of U-profile substrate and bottom row shows front- (left), back- (centre) and side- (right) view of U-profile. Thickly coated regions are colored in red while uncoated regions are colored in blue. See also [27].

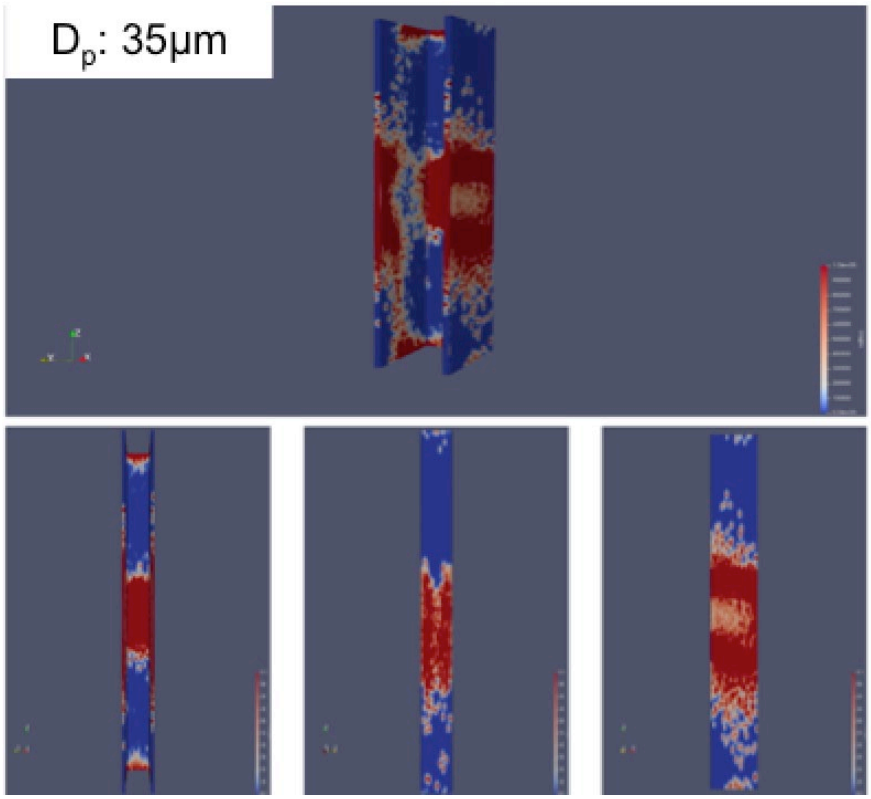

Figure 7b. Simulated coating patterns (visualization of Volume fraction fields) after single-burst-powder application for Mean particle diameter: 35µm. Top row shows front-side view of U-profile substrate and bottom row shows front- (left), back- (centre) and side- (right) view of U-profile. Thickly coated regions are colored in red while uncoated regions are colored in blue. See also [27].

The combined results of all 100 simulation-runs, depicted in Figure 8, show that the maximum Coating efficiency can be achieved at Mean particle diameters of 35µm +/-2µm. The minimum Relative Standard batch-based coating deviation or maximum homogeneity is located at Mean particle diameters of 25µm +/-2µm. The provided uncertainty of +/-2µm comes from the grid spacing of the conducted parameter study and does not represent the result of full numerical uncertainty quantification.

3.2. Plausibility Checks

Figures 7a, 7b and 7c allow qualitative plausibility checks of the achieved results.

In that respect, a comparison of coating patterns between Figure 7a (Mean particle diameter 5µm; minimum investigated diameter) and Figure 7b (Mean particle diameter 35µm; maximum Coating efficiency) reveals qualitatively similar formations. However, at 35µm, respective heavily coated regions appear generally enlarged, specifically at the backside and at the lateral protrusion. This prediction is highly plausible in light of Figure 9 as previously published in [4], which points out the qualitatively dominating force-effects on particle motion

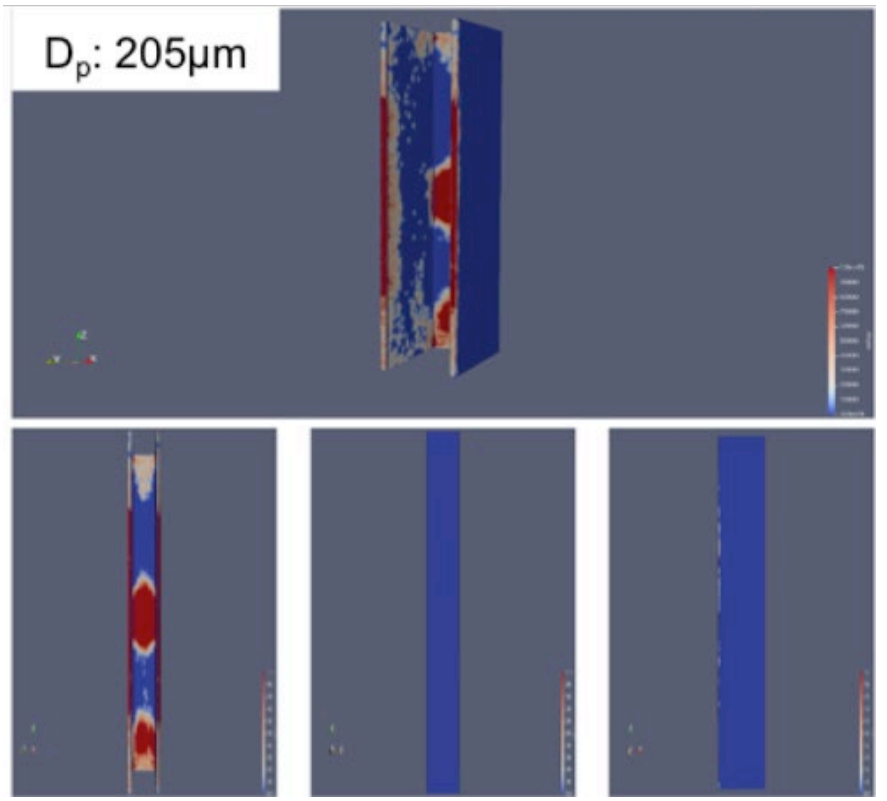

Figure 7c. Simulated coating patterns (visualization of Volume fraction fields) after single-burst-powder application for Mean particle diameter: 205µm. Top row shows front-side view of U-profile substrate and bottom row shows front- (left), back- (centre) and side- (right) view of U-profile. Thickly coated regions are coloured in red while uncoated regions are coloured in blue. See also [27].

and deposition within an exemplary powder coating scenario. In particular Figure 9 points out that for small ($D_p < 20\mu m$) particles fluid drag forces would dominate, whereas for medium sized ($20\mu m < D_p < 230\mu m$) particles, electrostatic forces would dominate the motion and deposition behavior. This is in line with the predicted patterns seen in Figures 7a and 7b such that 35µm particles would be more prone to electrostatic attraction than 5µm particles and thus would rather stick towards the lateral protrusion and to the backside than their smaller counterparts. Likewise, the stronger impact of fluid drag on the behaviour of 5µm particles as compared to 35µm particles would explain them getting dragged past the lateral protrusion and them not reversing as readily due to electro static forces towards the back side.

Predicted coating patterns according to Figure 7c (Mean particle diameter 205µm; maximum investigated diameter) are quite plausible as well. A comparison to the results for smaller particles as in Figures 7a and 7b, reveals much lower coating density at the backside as well as at the lateral protrusion. This is in line with the fact that large particles would not just tend towards gravitational dominance according to Figure 9, but would also feature much higher inertia. High inertia would cause these particles to practically shoot past the substrate,

once missed in the first place, yielding no chance to coat the backside nor the lateral protrusion of the U-profile.

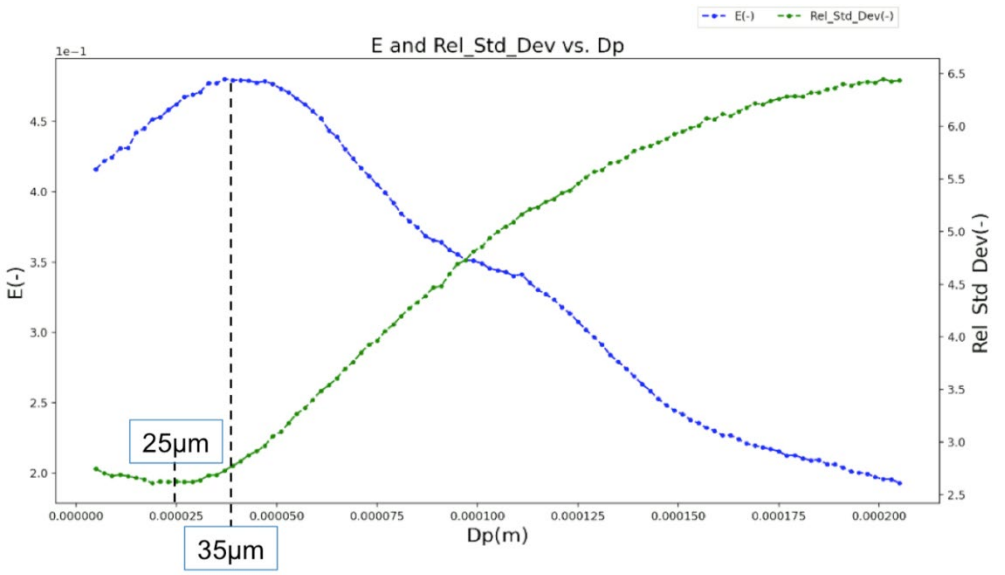

Figure 8. Combined results of 100 individual simulation runs where Mean particle diameters were varied in 100 steps between 5µm and 205µm. Coating efficiency (E, blue) and Relative Standard batch-based coating deviation (Rel_Std_Dev(-), green) against Mean particle diameters (D_p). See also [27].

3.3. Predicting the Impact of varying Powder Material Parameters: Standard deviation of particle diameters

This section presents the results of simulation-based predictions of the impact of varying Standard deviation of particle diameters σ_p on i) coating patterns (see Figure 10), ii) Coating efficiencies (see Figure 11, blue) and iii) relative standard batch-based coating deviation (see Figure 11, green) of a powder coated U-profile substrate. While the Standard deviation of particle diameters was varied in 100 steps between 5µm and 55µm, process- and material-parameters were fixed as follows: applied voltage: 50kV, distance pistol-substrate: 15cm, process airflow rate: $2m^3/h$, Mean particle diameters in Gaussian particle size distribution: 35µm, Particle density: 1400 kg/m^3.

The combined results of all 100 simulation-runs, depicted in Figure 11, show that the maximum Coating efficiency can be achieved at Standard deviation of particle diameters of 16.0µm +/-0.5µm. Furthermore, the minimum relative Standard batch-based coating deviation or maximum homogeneity is located at a Standard deviation of particle diameters of 10.5µm +/-0.5µm. The provided uncertainty of +/-0.5µm comes from the grid spacing of the conducted parameter study and does not represent the result of full numerical uncertainty quantification.

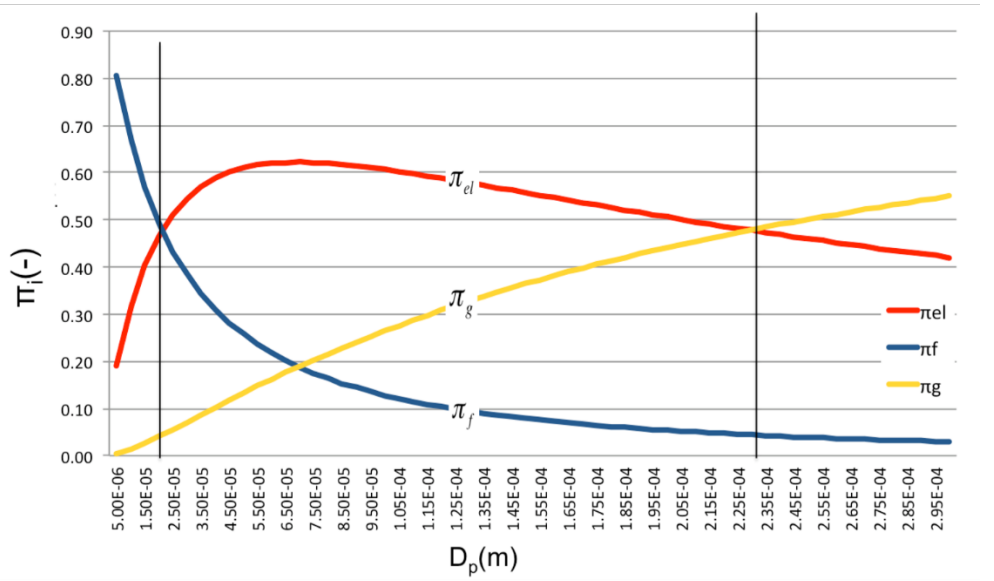

Figure 9. Dimensionless particle forces π i against particle diameter Dp. $D_p < 20\mu m$: dominance of ratio of fluid drag force to total force (blue); $20\mu m < D_p < 230\mu m$: dominance of ratio of electric forces to total force; $D_p > 230\mu m$: dominance of ratio of gravity force to total force. Representative case: Particle density $\rho_p = 1300 kg/m^3$, characteristic specific particle surface charge $q_p = 1C/m^2$, characteristic airflow velocity $v_{p,a} = 0.1m/s$, characteristic electrical field strength $E_{\max} = 0.75\, N/C$, dynamic viscosity of process air $\mu_a = 1.98 \times 10^{-5}\, Pa\, s$. For details see [4].

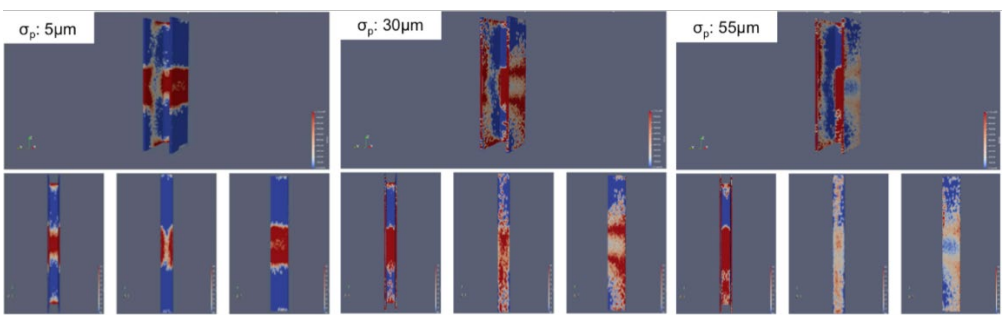

Figure 10. Simulated coating patterns (visualization of Volume fraction fields) for varying Standard deviation of particle diameters: 5µm (left), 30µm (centre) and 55µm (right). Top row shows front-side view of U-profile substrate and bottom row shows front- (left), back - (centre) and side - (right) view of U-profile per Standard deviation of particle diameters setting.

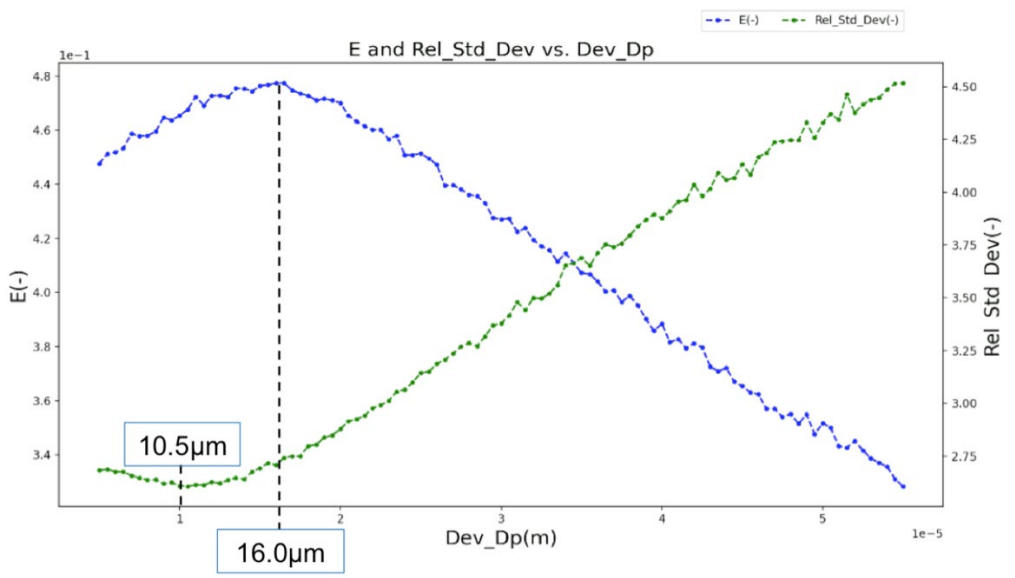

Figure 11. Combined results of 100 individual simulation runs where Standard deviation of particle diameters was varied in 100 steps between 5µm and 55µm. Coating efficiency (E, blue) and relative Standard batch-based coating deviation (Rel_Std_Dev, green) against Standard deviation of particle diameters (Dev_Dp).

3.4. Predicting the Impact of varying Powder Material Parameters: Particle density

This section presents the results of simulation-based predictions of the impact of varying Particle density ρ_p on i) coating patterns (see Figure 12), ii) Coating Efficiencies (see Figure 13, blue) and iii) Relative Standard batch-based coating deviation (see Figure 13, green) of a powder coated U-profile substrate. While the Particle density was varied in 100 steps between $500kg/m^3$ and $3500kg/m^3$, process- and material-parameters were fixed as follows: applied voltage: $50kV$, distance pistol-substrate: $15cm$, process airflow rate: $2m^3/h$, Mean particle diameter in Gaussian particle size distribution: 35µm, Standard deviation of particle diameters in Gaussian particle size distribution: $+/-16\mu m$.

The combined results of all 100 simulation-runs, depicted in Figure 13, show that the maximum Coating efficiency will be higher the lower the powder Particle density is. This result does not come as a surprise since, for increasing particle density, the ratio of acting fluid drag forces to electrostatic forces on the particle motion and deposition remains unchanged, while gravitational force and inertial effects increase. For medium sized particles, the latter two effects will always lead to a decrease of Coating efficiency. Thus, the achieved results for predicted Coating efficiencies under varying Particle densities could also be interpreted as additional plausibility checks of the simulation.

However, the simulated results for the relative Standard batch-based coating deviation are non-trivial and do provide added knowledge. In particular the results show that a minimum relative or maximum homogeneity can be located at a Particle density of $850kg/m^3$ $+/-30kg/m^3$.

The provided uncertainty of $+/-30kg/m^3$ comes from the grid spacing of the conducted parameter study and does not represent the result of full numerical uncertainty quantification.

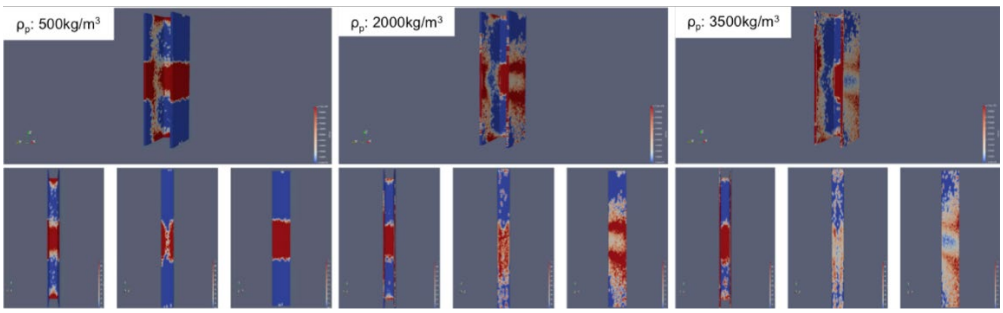

Figure 12. Simulated coating patterns (visualization of Volume fraction fields) for varying Particle densities: $500kg/m^3$ (left), $2000kg/m^3$ (centre) and $3500kg/m^3$ (right). Top row shows front-side view of U-profile substrate and bottom row shows front- (left), back- (centre) and side- (right) view of U-profile per powder Particle density setting.

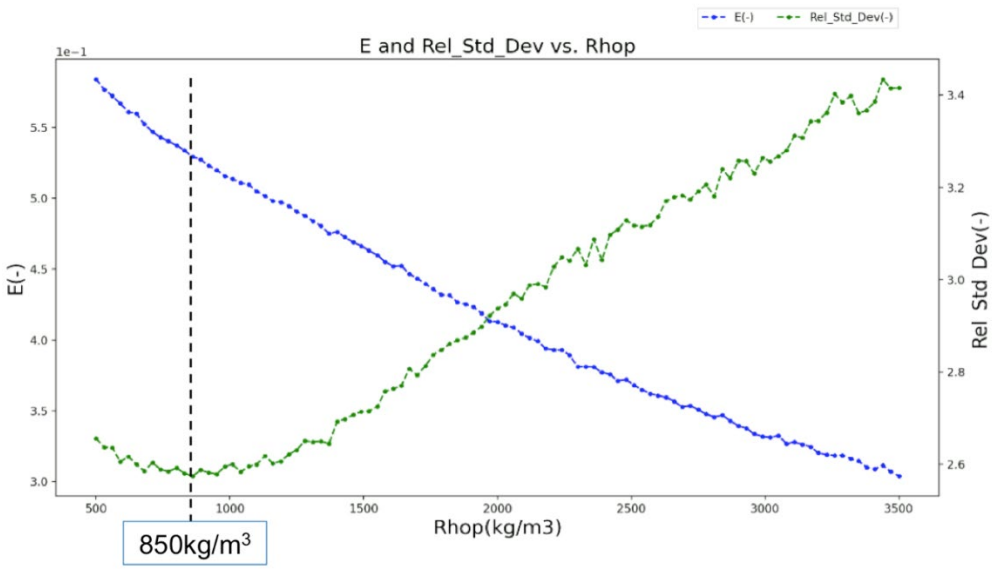

Figure 13. Combined results of 100 individual simulation runs where Particle density was varied in 100 steps between $500kg/m^3$ and $3500kg/m^3$. Coating efficiency (E, blue) and relative Standard batch-based coating deviation (Rel_Std_Dev, green) against Particle density (Rhop).

4. CONCLUSION AND OUTLOOK

A validated solver for powder-coating processes was introduced in this study. The solver, based on OpenFOAM and Euler-Lagrangian numerical methods, can accurately predict the most important performance characteristics of the powder coating process in relation to applied process parameters. Specifically, this study investigated the effect of varying coating powder material parameters, including Mean particle diameters, Standard deviation of particle diameters, and powder Particle density, on the coating results of a representative metallic U-profile substrate. The key-performance-attributes of the coating process, including coating patterns, coating efficiencies, and standard batch-based coating deviations, were also predicted using the solver.

To conduct the simulation-based parameter studies, the solver was made compatible with Kaleidosim Massive Simultaneous Cloud Computing technology. Three large studies were performed, each consisting of 100 individual simulation runs, one for each of the powder parameters. By executing batches of 100 simulation runs simultaneously in the cloud, the waiting time for completing the studies was reduced to only 120% of the execution time of one single simulation run.

While the study was limited to a static pistol-substrate set-up and a single-particle-burst-application, the results obtained are still practically useful for the coating of U-profiles in general. Although parameter-cross-dependencies were not investigated, the comparison of relative process-performance in a static, single-burst scenario is indicative of the performance in any possible, more complex process scenario. This implies that the better-performing set of powder-parameters in a static, single-burst scenario is likely to perform better in a more complex process scenario, where multiple pistols may be moved with varying speeds, orientation, and/or powder injection patterns.

In particular the presented study points to the fact that clearly distinguishable optima of all three powder-parameters can be found both in terms of Coating efficiency and in terms of Coating homogeneity. For otherwise typical process conditions, namely 50kV applied voltage, 15cm pistol-substrate-distance, 0° relative azimuthal substrate rotation, $2m^3/h$ primary process airflow and pending above stated limitations, the optima of Coating efficiency and Coating homogeneity were identified as seen in Table 1.

Table 1: Summary of optimum powder material parameters in terms of Coating efficiency and Coating homogeneity, as retrieved by simulations.

	Mean particle diameter [27]	**Std. Deviation of Particle Diameters**	**Particle Density**
Optimum Coating efficiency	35.0µm +/- 2µm	16.0µm +/- 0.5µm	the lower the better
Optimum Coating homogeneity	25.0µm +/- 2µm	10.5µm +/-0.5µm	850kg/m^3 +/-30kg/m^3

Table 1 presents clear guidelines for the knowledge-based design of powder materials for U-profile applications, and the authors believe that the outcomes have the potential to improve the quality of U-profile powder-coating applications while reducing resource intensity compared to the current state-of-the-art.

Nevertheless, further research in this field is required because only a limited subset of the U-profile powder-coating design-space could be covered in this study, despite conducting approximately 300 simulation runs. Geometric parameters, such as U-profile geometry, pistol-substrate distance or orientation, process parameters such as applied voltage or process air-flow-rates, and environmental parameters, such as humidity, were kept at "reasonably common" values. A full-factorial analysis of these additional degrees of freedom, including their cross-dependencies, would require millions of predictive simulation runs. While the current simulation technology is a considerable step forward in knowledge-based powder-coating-line-adjustments, the next level of technology is already under development. It will focus on surrogate modelling and have the potential to address the vast process-design-space.

REFERENCES

[1] Weller, H.G.; Tabor, G.; Jasak, H.; Fureby, C. (1998). A tensorial approach to computational continuum mechanics using object-oriented techniques. Computers in Physics, 12(6), 620.

[2] Boiger, G.; Boldrini, M.; Lienhard, V.; Siyahhan, B.; Khawaja, H.; Moatamedi, M. (2019). Multiphysics Eulerian-Lagrangian Electrostatic Particle Spray- And Deposition Model for OpenFoam® and KaleidoSim® Cloud-Platform (2020). International Journal of Multiphysics, 14(1), 1-15.

[3] Siyahhan, B.; Boldrini, M.; Hauri, S.; Reinke, N.; Boiger, G. (2018). Procedure for experimental data assessment for numerical solver validation in the context of model-based prediction of powder coating patterns (2019). International Journal of Multiphysics, 12(4), 373-392.

[4] Boiger, G. (2016). Characterization of particle-laden flows and deposition behavior in electrostatic fields. International Journal of Multiphysics, 10(2), 195–204(10).

[5] Boiger, G. (2016). Eulerian-LaGrangian model of particle-laden flows and deposition effects in electrostatic fields based on OpenFoam. International Journal of Multiphysics, 10(2), 177–194(8).

[6] Boiger, G., Sharman, D., Siyahhan, B., Lienhard, V., Boldrini, M., & Drew, D. (2021). A massive simultaneous cloud-computing platform for OpenFOAM. 9th OpenFOAM Conference, online, 19-20 October 2021.

[7] Boiger, G., Sharman, D., & Drew, D. (2021). KaleidoSim: massive simultaneous cloud computing for multiphysics simulations. In Multiphysics 2021. International Conference of Multiphysics, Online, 9-10 December 2021. International Society of Multiphysics, pp. 29. ISSN (online) 2409-1669.

[8] Boiger, G., Everitt, M., Sharman, D., & Boldrini, M. (2020). Massive simultaneous cloud computing (MSCC) for multiphysics-simulation applications. In Multiphysics 2020. International Conference of Multiphysics, Online, 11-12 December 2020. International Society of Multiphysics, pp. 59. ISSN (online) 2409-1669.

[9] Boiger, G., Buff, V., Sharman, D., Boldrini, M., Lienhard, V., & Dominic, D. (2020). Simulation-based investigation of tar formation in after-treatment systems for biomass gasification. Biomass Conversion and Biorefinery, pp. 1-18.

[10] Marmet, Ph., Holzer, L., Hocker, T., Boiger, G., Hilden, J., Reeb, S., & Fingerle, M. (2021). Generation of virtual three-phase structures based on Gaussian random fields: An important option for Digital Materials Design of solid oxide fuel cell electrodes. In GeoDict User Meeting 2021 Book of Abstracts (pp. 22). Math2Market.

[11] Boiger, G., Mataln, M., & Brandstätter, W. (2009). Adaptive time stepping for explicit Euler implementation of spherical and non-spherical particle speed up. International Journal of Multiphysics, 3(3), 267-291(25).

[12] Boiger, G. (2009). Development and verification of a large, Lagrangian (non-)spherical dirt particle and deposition model to simulate filtration processes using OpenFOAM® (PhD thesis). Montanuniversität Leoben, Austria. ICE Strömungsforschung GmbH.

[13] Boiger, G., Mataln, M., & Brandstätter, W. (2009). Simulation of Particle Filtration Processes in Deformable Media, Part 3.2: Interaction modelling and solver verification of a non-spherical dirt particle solver. International Journal of Multiphysics, 3(4), 433-454(22).

[14] Boiger, G., Mataln, M., & Brandstätter, W. (2009). Simulation of Particle Filtration Processes in Deformable Media, Part 3.1: Basic concepts and particle-fluid force implementation of a non-spherical dirt particle solver. International Journal of Multiphysics, 3(4), 407-232(26).

[15] Boiger, G., Mataln, M., Brandstätter, W., & Gschaider, B. (2008). Simulation of Particle Filtration Processes in Deformable Media, Part 2: Large Particle Modelling. International Journal of Multiphysics, 2(2), 191-206(16).

[16] Boiger, G., Khawaja, H., & Moatamedi, M. (2020). Chapter 5 - Introduction: Large, (non-)spherical particle modelling in the context of fluid filtration applications. In Multiphysics Modelling of Fluid-Particulate Systems (Elsevier Academic Press London).

[17] Boiger, G., Khawaja, H., & Moatamedi, M. (2020). Chapter 6 - Methodology: Large (non-)spherical particle modelling in the context of fluid filtration applications. In Multiphysics Modelling of Fluid-Particulate Systems (Elsevier Academic Press London).

[18] Boiger, G., Khawaja, H., & Moatamedi, M. (2020). Chapter 7 - Validation: Experimental and semi-analytical validation (in the context of Large (non-)spherical particle modelling for fluid filtration applications). In Multiphysics Modelling of Fluid-Particulate Systems. Elsevier Academic Press London.

[19] Boiger, G., Khawaja, H., & Moatamedi, M. (2020). Chapter 8 - Application and results: Filter fibre engineering (in the context of Large (non-)spherical particle modelling for fluid filtration applications). In Multiphysics Modelling of Fluid-Particulate Systems. Elsevier Academic Press London.

[20] Boiger, G., Khawaja, H. and Moatamedi, M. (2020) 'Chapter 9 - Conclusion and Vision (in the context of Large (non-)spherical particle modelling for fluid filtration applications)', in Multiphysics Modelling of Fluid-Particulate Systems. Elsevier Academic Press London, 2020, pp. 287-304.

[21] Bouwman, M., Boiger, G. and Brandstätter, W. (2016) Multiphase simulations of a Lyocell process, Vol. 1. Saarbrücken: LAP Lambert Academic Publishing. ISBN 978-3-659-89583-8.

[22] Du, Z., Wen, S., Wang, J., Yin, C., Yu, D. and Luo, J. (2016) 'The Review of Powder Coatings', Journal of Materials Science and Chemical Engineering, Vol. 04, pp.54-59.

[23] Fortune Business Insights. (2022) 'Paints and Coatings Market Size, Share & Industry Analysis, By Resin (Epoxy, Acrylic, Polyester, Alkyd, PU, and Others), By Technology (Waterborne, Solventborne, Powder, and Others), By Application (Architectural, Automotive OEM, Marine, Coil, General Industrial, Protective Coatings, Automotive Refinish, and Others), and Regional Forecast, 2022-2029', Fortune Business Insights.

[24] Boiger, G., Boldrini, M. and Siyahhan, B. (2018) 'Enhancing the understanding of complex phenomena in powder coating, by applying Eulerian-Lagrangian simulation methodology', in Multiphysics 2018: International Conference of Multiphysics, Krakow, 13-14 December 2018, International Society of Multiphysics, pp. 26. ISSN (online) 2409-1669.

[25] Boiger, G. K. (2018) 'Eliminating anomalies of CFD model results of the powder coating process by refining aerodynamic flow-particle interaction and by introducing a dynamic particle charging model', in Scientific tracks & abstracts: Day 1, 3rd International Conference on Fluid Dynamics & Aerodynamics, Berlin, October 25-26, 2018.

[26] Bariska, A., Reinke, N. (2011) 'Berührungslose thermische Schichtprüfung', Swiss Engineering STZ, 57(16), School of Engineering, Zurich University of Applied Sciences (ZHAW), Winterthur, Switzerland.

[27] Boiger, G. and Siyahhan, B. (2022) 'Simulation-based Study of the Impact of Mean Powder Particle Diameters on Key-Performance-Attributes of the Powder Coating of U-Profiles Multiphase CFD', in Proceedings of the 20th International Conference of Numerical Analysis and Applied Mathematics (ICNAAM 2022), Heraklion, Crete, Greece, 19-25 September 2022, Accepted Manuscript Conference Proceedings.